

Measuring Ambient Densities and Lorentz Factors of Gamma-Ray Bursts from GeV and Optical Observations

Romain Hascoët, Indrek Vurm, Andrei M. Beloborodov

Physics Department and Columbia Astrophysics Laboratory, Columbia University, 538 West 120th Street New York, NY 10027

ABSTRACT

Fermi satellite discovered that cosmological gamma-ray bursts (GRBs) are accompanied by long GeV flashes. In two GRBs, an optical counterpart of the GeV flash has been detected. Recent work suggests that the GeV+optical flash is emitted by the external blast wave from the explosion in a medium loaded with copious e^\pm pairs. The full light curve of the flash is predicted by a first-principle radiative transfer simulation and can be tested against observations. Here we examine a sample of 7 bursts with best GeV+optical data and test the model. We find that the observed light curves are in agreement with the theoretical predictions and allow us to measure three parameters for each burst: the Lorentz factor of the explosion, its isotropic kinetic energy, and the external density. With one possible exception of GRB 090510 (which is the only short burst in the sample) the ambient medium is consistent with a wind from a Wolf-Rayet progenitor. The wind density parameter $A = \rho r^2$ varies in the sample around $10^{11} \text{ g cm}^{-1}$. The initial Lorentz factor of the blast wave varies from 200 to 540 and correlates with the burst luminosity. Radiative efficiency of the prompt emission in the sample is between 0.1 and 0.8. For the two bursts with detected optical flash, GRB 120711A and GRB 130427A, we also estimate the magnetization of the external blast wave. Remarkably, the model reproduces the entire optical light curve of GRB 120711A (with its sharp peak, fast decay, plateau, and break) as well as the GeV data. The spectrum of GeV flashes is predicted to extend above 0.1 TeV, where they can be detected by ground-based Cherenkov telescopes.

Subject headings: plasmas – radiative transfer – plasmas – gamma-ray burst: general

1. Introduction

Cosmological gamma-ray bursts (GRBs) radiate most of their energy in the soft gamma-ray band between 100 keV and 10 MeV (Goldstein et al. 2012; Ackermann et al. 2013b). The MeV burst typically lasts seconds or minutes and is then followed by broad-band afterglow emission, which is associated with the deceleration of the explosion ejecta by the ambient medium (Mészáros & Rees 1997). Afterglow observations can be used to estimate the main parameters of

the GRB explosion — its Lorentz factor, kinetic energy, and the density of the ambient medium. Interpretation of observations became, however, challenging after the *Swift* satellite discovered bizarre X-ray and optical light curves of the early afterglow (Gehrels et al. 2009). *Swift* observations challenge the standard assumption that afterglow is emitted by the decelerating shock wave in the external medium; instead, it was proposed that afterglow is produced by a long-lived reverse shock (Uhm & Beloborodov 2007; Genet et al. 2007). Disentangling the two possible mechanisms is difficult, and a reliable method for deducing the explosion parameters from observations has been lacking.

The discovery of GeV flashes by the *Fermi* satellite opens a new way for solving this problem. The observed flashes have similar light curves with a special shape: they begin with a delay and sharply peak well before the end of the MeV burst; then the light curve exhibits a long gradual decay (Ackermann et al. 2013b). It is natural to associate the extended GeV emission with the external blast wave (Zou et al. 2009; Kumar & Barniol Duran 2009; Ghisellini et al. 2010) although this scenario faced difficulties in explaining the early peak of the GeV flash (Gao et al. 2009; He et al. 2011; Maxham et al. 2011). The puzzling peak was recently explained by the exponential e^\pm loading of the external medium by the prompt MeV radiation ahead of the blast wave (Beloborodov et al. 2014). Since the radius of pair loading is well defined and can be determined from the prompt GRB observations, the GeV flash provides a standard “ruler” and a unique opportunity for disentangling the explosion parameters. Detailed modeling of the pair-loaded blast wave was performed for GRB 080916C (Beloborodov et al. 2014) and GRB 130427A (Vurm et al. 2014). It was shown that the GeV flash is emitted by the *thermal* plasma heated in the forward shock, which is cooled by inverse Compton (IC) scattering of photons of lower energies.

Along with the IC flash, the blast wave should emit synchrotron radiation, in particular in the optical band. Pair loading shapes the optical synchrotron light curve similarly to the IC GeV flash. As a result, the model predicts an optical flash with a sharp peak at a time close to the GeV peak. Following the peak, the optical emission should quickly decay, as the pair-loading effect is reduced, and the steep decay should be followed by a flatter light curve of the normal pair-free afterglow. The predicted GeV+optical flash has been detected in GRB 130427A (Vestrand et al. 2014), and the radiative transfer simulation of Vurm et al. (2014) reproduced both the GeV and optical light curves of the flash.

The consistency of the model with the data is remarkable given the fact that it has only four adjustable parameters: (1) the ambient wind density parameter $A = \rho R^2$, (2) the explosion Lorentz factor Γ_{ej} , (3) the prompt emission efficiency $\epsilon_{\text{rad}} = E_{\text{GRB}}/(E_{\text{GRB}} + E_{\text{ej}})$, which determines the isotropic kinetic energy of the explosion E_{ej} for a GRB with observed isotropic energy E_{GRB} , and (4) the magnetization of the blast wave ϵ_B . This fourth parameter only enters the calculation of the optical light curve and does not affect the GeV flash; therefore, the model of GeV emission has only three adjustable parameters. Other parameters of the explosion, e.g. the deceleration radius R_{dec} and the pair loading factor $Z_\pm(R)$, are not adjustable — they are calculated from the blast wave dynamics and the observed prompt radiation.

In this paper, we investigate all observed GRBs with well measured light curves of the flash. Our goal is to further test the proposed model and, if the model fits the data, to determine the parameters of the GRB explosions. We perform radiative transfer calculations individually for each burst, search for a blast wave model that would be able to reproduce the observed light curves of GeV emission and, if data is available, optical. Section 2 describes the sample of GRBs, and Section 3 describes the model and the method of our analysis. The results are presented in Section 4 and further discussed in Section 5.

2. GRB sample

The choice of bursts for our sample is based on two criteria: (1) good *Fermi* LAT data, which provide the shape of the GeV flash, and (2) measured cosmological redshift z . In addition, we looked for bursts with available early optical data. We identified seven GRBs useful for our analysis: 080916C, 090510, 090902B, 090926A, 110731A, 120711A, and 130427A.

The *Fermi* LAT data are taken from the published LAT catalogue (Ackermann et al. 2013b) for GRBs 080916C, 090510, 090902B, 090926A, 110731A. Two recent GRBs 120711A and 130427A are not in the catalogue; their published LAT and optical flash data are taken from Ackermann et al. (2014), Martin-Carrillo et al. (2014), and Vestrand et al. (2014).

The prompt radiation data (which are used as an input of our transfer simulations) are from Abdo et al. (2009b) for GRB 080916C, Ackermann et al. (2010) for GRB 090510, Abdo et al. (2009a) for GRB 090902B, Ackermann et al. (2011) for GRB 090926A, Ackermann et al. (2013a) for GRB 110731A, and Gruber & Pelassa (2012) for GRB 120711A. The prompt data for GRB 130427A are taken from Golenetskii et al. (2013); Ackermann et al. (2014). These papers provide an approximate description of the spectral evolution in each GRB, using spectral fits in temporal bins. This evolution is useful to take into account in our transfer simulations, however its details are not essential and weakly affect the results. For instance, in GRB 090510 it is safe to neglect the small precursor, as it carries small energy. In GRB 110731A we merged the first two time bins “A” and “B” into a single bin to smoothen the jumps in luminosity and spectral parameters reported by Ackermann et al. (2013a). These jumps mostly result from two different ways of fitting the observed spectrum: bin A spectrum was fitted by a power law with an exponential cutoff while bin B spectrum was fitted by a Band function whose high-energy slope is affected by the inclusion of the LAT data (see Ackermann et al. 2013a).¹

The optical and X-ray afterglow data are from Greiner et al. (2009) for GRB 080916C, De Pasquale et al. (2010) for GRB 090510, Pandey et al. (2010) for GRB 090902B, Swenson et al. (2010) for GRB 090926A, Ackermann et al. (2013a) for GRB 110731A, Martin-Carrillo et al. (2014) for GRB 120711A, and

¹The inclusion of GeV data in the Band component can be dangerous, as the GeV signal contains a separate component from the external blast wave, which can corrupt the inferred parameters of the Band MeV spectrum.

Vestrand et al. (2014) for GRB 130427A. We use the afterglow data to estimate the soft radiation field in the source, which dominates the IC cooling of the blast wave after the prompt MeV radiation. The afterglow reconstruction uses the simple power-law interpolation of the observed spectra and light curves. Extrapolation of the available data to earlier times was needed for several bursts. The disadvantage of this method is that the accuracy of the simple power-law extrapolation is uncertain, in particular for GRBs 090510, 080916C, 090902B, and 090926A. The advantage is that the method is well defined, model-independent, and minimizes special treatment of bursts with incomplete afterglow data. Fortunately, the rough reconstruction of the target soft radiation for IC scattering does not create large uncertainties in the light curve of the predicted GeV flash. In particular, in the fast cooling regime, the details of the target spectrum play almost no role (Beloborodov et al. 2014).

3. The model

Pair loading of the external medium by the MeV radiation can be accurately calculated for any observed GRB with a known redshift, using the observed luminosity (isotropic equivalent) and spectrum of the prompt radiation. For any optically thin medium, the pair loading factor $Z_{\pm} = n_{\pm}/n$ does not depend on the medium density n , and is only a function of radius R (Thompson & Madau 2000; Beloborodov 2002). The function $Z_{\pm}(R)$ is obtained by solving radiative transfer for the prompt MeV radiation. The transfer weakly affects the observed prompt radiation, however it strongly impacts the medium by depositing momentum and creating new particles. The pair loading factor is huge at small radii, $Z_{\pm} \sim 10^4 - 10^5$, and is steeply reduced outside a characteristic “pair-loading” radius. The fast evolution of the e^{\pm} density shapes the peak of the GeV flash and its initial decay, as described in detail in Beloborodov et al. (2014). For a typical bright burst observed by *Fermi* LAT, the peak radius R_p is comparable to 10^{16} cm. It is smaller than the deceleration radius of the blast wave, R_{dec} , and therefore the GeV flash peaks before the onset of normal afterglow, which is shaped by the blast wave deceleration.

The mechanism of the GeV flash may be summarized as follows. The blast wave has a high Lorentz factor Γ and heats the pair-loaded external medium to a relativistic temperature. The medium is cooled behind the shock via inverse Compton (IC) and synchrotron emission. IC cooling is extremely fast as long as the blast wave is exposed to the prompt MeV radiation (which is produced at much smaller radii and gradually overtakes the blast wave, with the relative speed of $\Delta v = c/2\Gamma^2$). When the prompt GRB radiation fully overtakes and decouples from the blast wave, the shock-heated plasma is cooled via the slower synchrotron-self-Compton (SSC) emission. The SSC regime occurs in the far tail of the GeV flash; the tail is well observed for some GRBs, in particular in GRB 130427A.

In contrast to the older concept that GeV emission comes from nonthermal particles accelerated in the shock, Beloborodov et al. (2014) showed that the main, *thermal* population produces GeV-TeV emission. Therefore a large fraction of the blast wave energy is radiated in the high-energy

bands. The thermal plasma also produces the synchrotron optical flash. Electrons/positrons injected with the thermal Lorentz factor γ_{th} strongly dominate synchrotron spectrum at frequencies $\nu < \nu_m \sim \Gamma \gamma_{\text{th}}^2 eB/m_e c$, which covers the optical band during the flash.

The dominance of radiation from the thermal plasma makes the model simple to test, without invoking phenomenological parameters describing the nonthermal tail. Nonthermal particles dominate synchrotron emission at $\nu > \nu_m$; this regime applies to the late optical afterglow when ν_m decreases below 10^{15} Hz. During the flash, $\nu > \nu_m$ only at high (X-ray) frequencies. An extended nonthermal tail of the electron distribution can produce synchrotron radiation from the X-ray band up to ~ 0.1 GeV, contributing to the flux detected by LAT. This radiation is, however, found to be negligible in our best-fit models of GeV flashes (except perhaps the special case of GRB 090510).² Therefore, effectively three parameters (Γ_{ej} , ϵ_{rad} , A) enter the fitting of the GeV flash, and ϵ_B is only relevant for the optical flash.

Nonthermal synchrotron radiation implicitly enters our flash model in a different way: it provides targets for IC scattering in the SSC tail of the GeV flash. Since the nonthermal synchrotron modeling is expensive (and uncertain, especially when the reverse shock contribution is included), we estimate the targets using the actual *observed* afterglow (Section 2).

The model must assume a value for the fraction ϵ_e of the shock energy that is given to the thermal electron/positron plasma. Beloborodov et al. (2014) showed that $\epsilon_e \approx 1$ during the peak of the flash. At later times (when Z_{\pm} drops to 500), ϵ_e is reduced to 0.3, a typical value reported by the simulations of collisionless shocks (Sironi & Spitkovsky 2011). Note that the thermal ϵ_e is much less uncertain than the corresponding parameter of nonthermal particles; it is frozen and taken the same for all bursts.

The progenitor wind has the mean molecular weight per electron $\mu_e = \rho/n_e m_p = 2$ (elements heavier than hydrogen). The correct choice of μ_e is essential in simulations of GRB afterglow (see the discussion in Vurm et al. 2014 and comparison with Panaitescu et al. 2013). GRB 090510 is a short GRB and a special case; therefore for this burst we also search for a solution with uniform external medium and $\mu_e = 1$.

Appendix A summarizes simplified analytical estimates for the theoretical GeV+optical flash, which demonstrate basic trends in the model. Deviations of the accurate simulations from the estimates highlight the importance of detailed calculations for each GRB individually, using as an input its observed prompt radiation. Below the model with adjustable parameters A , Γ_{ej} , ϵ_{rad} (and ϵ_B , if optical flash data is available) is calculated for each GRB and fitted to the data. The calculation involves a careful radiative transfer simulation, as described in detail in Beloborodov et al. (2014). The simulation is expensive and we do not attempt a formal fitting of the data that would give χ^2 for the best fit. Instead, we manually search the parameter space for an acceptable solution.

²During the peak of the flash, synchrotron cooling of the blast wave is negligible compared with IC cooling (as long as $\epsilon_B \ll 0.1$). It remains negligible in the tail if $\epsilon_B \ll 10^{-3}$.

Table 1: Three main observational parameters of the GRBs in our sample and four adjustable parameters of the model. E_{GRB} – prompt radiation energy (isotropic equivalent), $T_{\text{GRB}} = T_{90}/(1+z)$ – redshift-corrected duration of the prompt emission, z – cosmological redshift. $A = \rho R^2$ – wind density parameter, Γ_{ej} – ejecta Lorentz factor, ϵ_{rad} – prompt efficiency, ϵ_B – magnetization.

GRB	E_{GRB} [10^{54} erg]	T_{GRB} [s]	z	A [10^{11} g/cm]	Γ_{ej}	ϵ_{rad}	ϵ_B
080916C	8.8	12	4.35	$1.5 \rightarrow 3.5$	$900 \rightarrow 1400$	0.17	–
090510	0.11	1.1	0.903	$1.2 \rightarrow 2$	$700 \rightarrow 800$	0.1	–
090510 (uniform)	–	–	–	$n = 2 \times 10^4 \text{ cm}^{-3}$	900	0.1	–
090902B	3.6	7.8	1.822	$1 \rightarrow 2$	$600 \rightarrow 900$	0.4	–
090926A	2.2	4.2	2.106	$1 \rightarrow 2$	$600 \rightarrow 1000$	0.25	–
110731A	0.76	1.9	2.83	$0.4 \rightarrow 0.8$	$800 \rightarrow 1100$	0.2	–
120711A	1.65	48	1.405	$1 \rightarrow 3$	$320 \rightarrow 400$	0.3	$10^{-5} \leftarrow 10^{-6}$
130427A	0.85	15	0.34	$0.15 \rightarrow 0.5$	$300 \rightarrow 350$	0.8	$10^{-3} \leftarrow 2 \times 10^{-4}$

Table 2: Other physical quantities calculated from the model: Γ_p – blast wave Lorentz factor at radius R_p of the GeV peak, R_{dec} – deceleration radius, R_{\pm} – pair loading radius, t_{sc} – time (measured in central engine frame) when the IC cooling of thermal electrons becomes inefficient.

GRB	Γ_p	R_p [10^{16} cm]	R_{dec} [10^{16} cm]	R_{\pm} [10^{16} cm]	t_{sc} [s]
080916C	540	1	$10 \leftarrow 6$	10	$200 \rightarrow 300$
090510	500	0.2	$0.35 \leftarrow 0.3$	0.9	$100 \rightarrow 200$
090510 (uniform)	400	0.2	0.3	0.9	$> 10^4$
090902B	300	1	$4 \leftarrow 3$	9	$6 \times 10^3 \rightarrow 3 \times 10^4$
090926A	390	1.1	$5 \leftarrow 4$	9	$1.5 \times 10^3 \rightarrow 6 \times 10^3$
110731A	540	0.5	$2.5 \leftarrow 2$	4	$600 \rightarrow 4 \times 10^3$
120711A	200	3	$10 \leftarrow 6$	12	$350 \rightarrow 10^3$
130427A	250	1	$3 \leftarrow 2.5$	6	$2 \times 10^3 \rightarrow 7 \times 10^3$

4. Results

For each GRB in the sample, the model successfully reproduced the observations in a narrow region of the parameter space, which allowed us to measure the parameters (Table 1). The theoretical light curves of the GeV and optical flashes are compared with observations in Figures 1-3. For each GRB, we found two solutions whose predictions for the LAT/optical flux differ by about 1σ . This gives a rough estimate of the “error bar” on the measured A and ϵ_B . A moderate uncertainty also results from the uncertain contribution of the prompt emission to the GeV light curve at early times, which is suggested by the variability in the observed light curve. It implies a somewhat lower peak of the smooth flash associated with the external blast wave.

In all seven GRBs the GeV peak occurs while the prompt emission is still going on. This fact alone shows that the GeV flash is not associated with the deceleration radius of the blast wave. Table 2 gives more details of the reconstructed explosion — Lorentz factor Γ_p and radius R_p of the

blast wave at the GeV peak, the deceleration radius R_{dec} , the pair loading radius R_{\pm} where Z_{\pm} drops below 2, and the (redshift-corrected) time t_{sc} when the cooling (synchrotron+IC) of thermal electrons becomes inefficient. We find $Z_{\pm}(R_p) \sim 10^3 - 10^4$, a robust feature of our model: pair loading of the external medium is responsible for the extremely efficient processing of shock energy into GeV gamma-rays, as explained in detail in Beloborodov et al. (2014).

The pair loading Z_{\pm} rapidly decreases during the peak and early decay of the GeV light curve; as a result, the shock energy *per lepton* increases and the characteristic IC photon energy sweeps across the GeV band. All the presented models show similar evolution of the flash spectrum: the spectrum is soft during the rise of the GeV flash, then quickly hardens and remains approximately flat ($\nu L_{\nu} \sim \text{constant}$) during the most luminous phase. This behavior is consistent with the spectral slopes observed by *Fermi* LAT (Ackermann et al. 2013b) (with one notable exception — GRB 090510, whose spectrum is softer, see Section 5.4). At later times the predicted spectrum slightly hardens, approaching $\nu L_{\nu} \propto \nu^{1/2}$ that characterizes emission from fast-cooling thermal electrons. The predicted behavior of the optical spectrum is similar: flat near the peak, followed by moderate hardening as the synchrotron frequency ν_m moves beyond the optical band. At present we possess no data on the spectral slope of the optical flash; its predicted behavior could be tested by future optical observations.

Figures 1-3 also show the predicted TeV emission to provide some guidance for future observations with Cherenkov telescopes. The characteristic IC photon energy reaches the TeV band in seconds or minutes after the GeV peak. The high-energy spectrum is most extended near the pair loading radius R_{\pm} ; the maximum photon energy is typically between a few hundred GeV and ten TeV, and scales as $E_{\text{kin}}/(AE_{\text{GRB}}^{1/2})$ where E_{kin} is the kinetic energy of the blast wave. The electrons behind the shock are still fast-cooling at this stage, and their bolometric IC luminosity is $\sim \epsilon_e E_{\text{kin}}/(4t)$. The flat (or even slightly rising) high-energy spectrum places a sizable fraction of this luminosity into the TeV band, resulting in comparable GeV and TeV fluxes. Our transfer simulations also show that the high-energy flash is partially absorbed by local photon-photon collisions. This intrinsic absorption is included in all GeV-TeV flash models presented in this paper, however the effect is never dramatic, because the flash always peaks where the radiation column density is reduced below a critical value (see Beloborodov et al. 2014 for a detailed discussion). In particular, intrinsic absorption does not create a break of the high-energy spectrum, although it does moderately affect the spectrum shape.

The TeV emission peaks immediately after its onset. Its decay is relatively slow, so that most of the energy above 0.1 TeV is emitted approximately over a decade in time after the peak, typically within a few minutes of the GRB trigger (Figures 1-3). The TeV flux from the thermal electrons behind the shock cuts off when the characteristic energy of the IC photons falls below 0.1 TeV, which typically occurs after a few hours or a day. An additional nonthermal electron population could affect the rise of the TeV light curve and extend the emission to later times, however it would not influence the most luminous phase.

The seed photon field for IC scattering significantly changes at the time when the prompt MeV radiation completely overtakes the blast wave, as the remaining X-ray and optical afterglow radiation is softer and less luminous. The theoretical GeV light curves show no special features at this transition (Figures 1-3). This is because the shock-heated plasma is still in the fast-cooling regime; therefore it produces the same IC emission regardless of the details of the target spectrum.

At the time of the GeV peak the ejecta kinetic energy is still being transferred to the blast wave via the reverse shock. Comparison of the ejecta and blast wave Lorentz factors in Tables 1 and 2 reveals that the reverse shock is at least mildly relativistic in most GRBs in the sample. When $\Gamma_{\text{ej}} \gg \Gamma$ (ultra-relativistic reverse shock), the blast wave dynamics and radiation are insensitive to Γ_{ej} . Then the model of the GeV flash effectively has only two parameters: A and ϵ_{rad} . The flash observations provide accurate estimates for the blast wave Lorentz factor Γ , however Γ_{ej} is more difficult to measure. In some cases, only lower limits on Γ_{ej} are obtained.

The relativistic reverse shock crosses the main part of the ejecta (carrying most of the explosion energy) in about the same time as it takes the prompt MeV radiation to fully overtake the blast wave. This time also corresponds to the observed time T_{90} and the deceleration radius R_{dec} . After this moment, the blast wave is approximately described by the Blandford-McKee self-similar solution. Note that $R_{\text{dec}} < R_{\pm}$ for all bursts in the sample, i.e. the effects of pair-loading continue to impact the afterglow emission for some time after the end of the prompt emission. This “memory” of pair creation is even more significant at low frequencies where the emission occurs in the slow-cooling regime (Beloborodov 2005).

5. Discussion

In this paper, we tested the GeV flash model proposed by Beloborodov et al. (2014) using a sample of GRBs which includes all bursts with good LAT data and known redshifts. All 7 bursts in the sample are intrinsically bright, with peak luminosities ranging from $\sim 10^{53}$ erg s $^{-1}$ (GRB 130427A) to $\sim 10^{54}$ erg s $^{-1}$ (GRB 080916C). We performed radiative transfer simulations for each of the 7 bursts. The input of the simulation is the observed prompt MeV radiation and the observed optical/X-ray afterglow, and the output is the GeV light curve. The model has three adjustable parameters: the Lorentz factor of the GRB ejecta Γ_{ej} , the ambient density parameter A , and the radiative efficiency of the prompt emission $\epsilon_{\text{rad}} = E_{\text{GRB}}/(E_{\text{GRB}} + E_{\text{ej}})$. We found that the model well explains the observed light curves in the sample. This allowed us to obtain estimates for Γ_{ej} , A , and ϵ_{rad} .

5.1. Ambient medium

Explosion into a wind-type medium is consistent with the observed flash for all GRBs in the sample except possibly GRB 090510 (see below). We found that the wind parameter A shows

moderate variations in the sample, between $0.15 \times 10^{11} \text{ g cm}^{-1}$ and $3.5 \times 10^{11} \text{ g cm}^{-1}$ (Table 1). These values are comparable with typical $A \sim 3 \times 10^{11} \text{ g cm}^{-1}$ estimated for the winds of Wolf-Rayet stars in our Galaxy (Crowther 2007). This result provides further support for the association of GRBs with collapse of Wolf-Rayet stars. Evidence for this association was previously provided by a few GRBs with a detected supernova counterpart of type Ib or Ic (Woosley & Bloom 2006).

We also note that the obtained values of A do not contradict the upper limits estimated by Hascoët et al. (2014) with a different method and for a different sample of bursts. In that work, the most constraining upper limits $A_{\text{max}} \sim 10^{11} \text{ g cm}^{-1}$ were obtained for GRBs with luminosities below $10^{52} \text{ erg s}^{-1}$ (Figure 4). Comparison of these upper limits with our estimates presented here suggests that the luminous bursts detected by LAT have systematically higher A .

In most bursts in the sample the flash peaks much earlier than the blast wave reaches the deceleration radius R_{dec} . In this situation, the models of uniform and wind external medium predict very different light curves of the flash, and we find that only the wind medium is consistent with the data. The distinction is less clear when R_p is comparable to R_{dec} . Then both the shape of the GeV peak and the decay of the light curve are relatively insensitive to the profile of the ambient medium (provided that the density at R_p remains similar and the emitting electrons are fast-cooling). In our sample, GRB 090510 falls into this category (see below). The separation between R_{dec} and R_p is also moderate in GRB 120711A and GRB 130427A, however the wind medium is still preferred in these two cases. Thus the wind medium is preferred by the analysis of all long bursts in the sample.

5.2. Lorentz factor

Measurement of GRB Lorentz factors is a long standing problem. Until recent work, the main method was based on estimates of photon-photon opacity for the gamma-rays detected by LAT, which gave lower limits on Γ_{ej} (e.g. Lithwick & Sari 2001; Granot et al. 2008; Hascoët et al. 2012).

Reconstruction of the GeV flash mechanism gives a valuable measurement of the Lorentz factor of the blast wave Γ *before its deceleration*, and also provides an estimate for the ejecta Lorentz factor $\Gamma_{\text{ej}} \gtrsim \Gamma$. This method was recently applied to GRB 080916C (Beloborodov et al. 2014) and GRB 130427A (Vurm et al. 2014). Our results extend this analysis to the sample of 7 GRBs. Figure 4 shows the obtained Lorentz factors versus the burst luminosity. We observe a positive correlation between Γ and the average luminosity of the GRB $L_{\text{GRB}} = E_{\text{GRB}}/T_{\text{GRB}}$, where the prompt burst energy E_{GRB} and its approximate duration T_{GRB} are given in Table 2. Provided that Γ_{ej} is not much higher than Γ (which is the case for GRB 130427A, and likely in the other bursts) we find a $L_{\text{GRB}}\text{-}\Gamma_{\text{ej}}$ correlation, which may be roughly approximated by a power-law relation $\Gamma_{\text{ej}} \approx 10^3 L_{54}^{1/2}$. Future observations of GeV flashes may allow a better measurement of this correlation.

There is another method of estimating Γ using the peak time of the optical afterglow (Liang et al.

2010; Ghirlanda et al. 2012). The method is based on the assumption that the peak is emitted at the deceleration radius of the blast wave. This assumption can be invalid for bright bursts which have large pair-loading radii (as demonstrated for the sample of GRBs studied in this paper); however it may be reasonable for less luminous bursts. A recent refinement of this method by Hascoët et al. (2014) gave measurements and upper limits for Γ in a large sample of bursts, which are included in Figure 4.³ They extend the $L_{\text{GRB}}-\Gamma$ diagram to lower luminosities $L_{\text{GRB}} < 10^{53} \text{ erg s}^{-1}$, however do not allow a reliable measurement of the correlation in this region because of the large number of lower limits. Overall, the data is consistent with the existence of a lower bound $\Gamma > \Gamma_{\text{min}}$ which increases with L_{GRB} . This bound may result from strong subphotospheric adiabatic cooling in explosions with $\Gamma_{\text{ej}} < \Gamma_{\text{min}}$ (see Hascoët et al. 2014).

We also note that within uncertainties our estimate for the jet Lorentz factor in GRB 130427A is in agreement with the value $\Gamma_{\text{ej}} = 450$ found from radiative transfer modeling of its prompt emission (Vurm & Beloborodov, in preparation).

5.3. Radiative efficiency

The inferred radiative efficiency ϵ_{rad} of the prompt GRB emission varies between 0.1 and 0.8 in the sample, i.e. $E_{\text{ej}}/E_{\text{GRB}} = 0.25 - 9$. Such high values of radiative efficiency may be expected. High ϵ_{rad} was previously suggested by the late afterglow analysis (e.g. Racusin et al. 2011) and also expected in theoretical models of the prompt emission (cf. Beloborodov 2010; Vurm & Beloborodov, in preparation).

5.4. The special case of GRB 090510

The IC cooling of shock-heated wind medium well explains the observed GeV flash for all GRBs in our sample except one: GRB 090510. In this case, the model rather well reproduces the peak of the flash at $t_{\text{obs}} \lesssim 1 \text{ s}$ and its initial decay at $t_{\text{obs}} < 10 \text{ s}$, however at $t_{\text{obs}} > 20 \text{ s}$ the theoretical emission falls short of the observed flux.

GRB 090510 is also special as the only short burst in our sample. Short GRBs are normally not associated with massive progenitors, although some of them may be “impostors” in the short class (the impostors are bursts that have a massive progenitor but happen to have short duration).

The deficiency of the theoretical GeV emission in GRB 090510 may be explained in two ways:

- (1) The ambient medium is not a wind from a massive progenitor. Indeed, we find that the

³ This method gives estimates for $\Gamma \rho_{\text{dec}}^{1/8}$ where ρ_{dec} is the density of the external medium at the deceleration radius. Therefore, there is a weak dependence of the inferred Γ on the assumed ρ_{dec} . In the left panel of Figure 4 we used $\rho_{\text{dec}} \sim 10^{-21} \text{ g cm}^{-3}$ which corresponds to $A \sim 10^{11} \text{ g cm}^{-1}$ and $R_{\text{dec}} \sim 10^{16} \text{ cm}$.

entire light curve of the GeV flash is reasonably well reproduced if the ambient density is uniform, $\rho \approx \text{const}$, rather than wind-like, $\rho \propto r^{-2}$. The uniform density must, however, be quite high, $n = \rho/m_p \sim 2 \times 10^4 \text{ cm}^{-3}$, well above the typical density of interstellar medium.

(2) An additional emission component is present in the flash observed by LAT. It can be synchrotron emission (extending to $E > 100 \text{ MeV}$) from nonthermal electrons accelerated in the blast wave. This interpretation is consistent with the relatively soft photon index ($\beta \sim 2.5 - 3$) measured for GRB 090510 at the time when the additional component dominates. Our simulation did not include possible nonthermal electrons because they are harder to model from first principles and require additional phenomenological parameters. We also note that the nonthermal component is not needed for the other 6 bursts — their GeV flashes are well explained by pure IC emission from the thermal plasma.

5.5. Optical flash

Two GRBs have a well measured optical counterpart of the GeV flash. The expected light curve of this (synchrotron) counterpart is obtained directly from the model of the GeV flash by introducing one additional parameter ϵ_B .

GRB 130427A has the best coverage in the LAT and optical bands. The entire GeV flash ($t < 1 \text{ d}$), and the main peak and steep decay of the optical flash ($t < 100 \text{ s}$), are well reproduced by the model of the pair-loaded forward shock. The optical light curve requires an additional contribution after 100 s, which we interpreted as emission from the reverse shock (Vurm et al. 2014). The forward shock produces the light curve similar to that observed in GRB 120711A (discussed below), with a plateau ending around 10^4 s . This plateau may be responsible for the hump in the optical light curve of GRB 130427A at $t \sim 10^4 \text{ s}$.

The result obtained for GRB 120711A is rather striking. The model reproduces the entire complicated optical light curve: the sharp rise at 30 s, the peak at 50 s, the steep decay between 50 and 300 s, the plateau and the break at 10^4 s . Our model has only four adjustable parameters A , ϵ_{rad} , Γ_{ej} , and ϵ_B . Such a remarkable fit of the optical light curve can hardly be obtained by chance. The same model also fits well the decay of the GeV flash, both the slope and the normalization. The GeV data are less constraining in this burst as the peak of the GeV flash was missed by LAT observations.

The inferred $\epsilon_B \sim 4 \times 10^{-4}$ for GRB 130427A and $\epsilon_B \sim 3 \times 10^{-6}$ for GRB 120711A give rough but reliable estimates for the characteristic magnetization in the external blast wave. In a more detailed model ϵ_B may be changing with time as discussed in Vurm et al. (2014). The excellent fit for GRB 120711A does not require such variation.

5.6. TeV emission

Our model predicts luminous TeV emission accompanying the GeV flash, which can be detected by ground-based Cherenkov telescopes. The bulk of the TeV fluence is accumulated within 1-10 minutes after the GRB trigger; the energy radiated above 0.1 TeV in the sample ranges from 10^{51} to 4×10^{53} erg, and constitutes up to 30% of the prompt MeV fluence.

The predicted efficiency of TeV emission varies substantially from burst to burst. For example, in GRB 120711A most of the energy above 100 MeV is radiated in the TeV band (Figure 3). In contrast, TeV emission is weak in the high- A (dense wind) models for GRB 090902B and GRB 090926A (Figure 1). The difference in the TeV flux arises mainly from the different maximal IC photon energy that the thermal electrons can produce, $E_{\max} \sim \Gamma \gamma_{\text{th}} m_e c^2$, where γ_{th} is the Lorentz factor of the thermal electrons behind the shock. In GRBs exploding into denser winds the blast wave is slower and loses a larger fraction of its kinetic energy at an early radiative stage. The reduced Γ gives a lower E_{\max} so that it may not exceed a few 100 GeV (in the GRB rest frame).

Nonthermal electrons can extend the IC emission above E_{\max} ; this emission was not included in our model, and thus the 0.1 TeV light curves shown in the figures should be viewed as a lower limit. The shock energy given to nonthermal electrons is small compared with the thermal population. Therefore, their presence in the 0.1 TeV light curve becomes important only when the contribution from the thermal electrons is suppressed, i.e. when $E_{\max} < 0.1$ TeV.

A major factor limiting the GRB detectability in the TeV band is the extinction by extragalactic background light (EBL). For example, at redshift $z = 1$ the attenuation factor is ~ 0.5 at 0.1 TeV and $\sim 5 \times 10^{-3}$ at 0.3 TeV (Domínguez et al. 2011; Gilmore et al. 2009). This leaves a narrow window between the Cherenkov detector threshold (presently $\sim 50 - 100$ GeV) and $\sim 0.2 - 0.3$ TeV for most bursts, except those that happen at unusually small z (such as GRB 130427A). As long as the intrinsic high-energy spectral cutoff is well above 100 GeV, the *observed* turnover would arise from the extragalactic absorption and could be used to place independent constraints on the EBL density.

The (approximate) low-energy threshold ~ 50 GeV, repositioning time of a few tens of seconds and sensitivity of the currently operating Imaging Atmospheric Cherenkov telescopes (IACT) such as MAGIC (Aleksić et al. 2012; Sitarek et al. 2013), VERITAS (Holder 2011; Kieda et al. 2013) and H.E.S.S. (Hinton & the HESS Collaboration 2004) would have been sufficient to detect at least two bursts in our sample: GRB 120711A and GRB 130427A. Their predicted fluxes above 0.1 TeV a few minutes after the GRB trigger are well above the sensitivity limit despite the substantial EBL absorption for GRB 120711A ($z = 1.405$). In the case of GRB 130427A ($z = 0.34$) the TeV emission remains at a detectable level for its entire duration, i.e. until the cutoff at a few $\times 10^4$ s. The cutoff is consistent with the upper limit provided by the VERITAS observation at 1 day (Aliu et al. 2014).

The projected sensitivity of the next generation Cherenkov Telescope Array (CTA) (Funk et al. 2013; Inoue et al. 2013) is sufficient to detect most of the bursts in our sample (including GRB

090510 if it exploded into a wind medium), with the possible exception of GRB 080916C and GRB 110731A owing to their high redshifts. Current efforts to reduce the energy threshold of the Cherenkov telescopes are key for future routine detection of high-energy GRB emission from the ground.

In this paper, we focused on the flash observations, and only in the bands where we think it is dominated by the thermal plasma behind the forward shock. The analysis of all afterglow observations, at all times and energies, from radio (Laskar et al. 2013) to hard X-rays (Kouveliotou et al. 2013) is deferred to future work. It will be significantly more involved, as it has to include the emission from nonthermal particles, from both reverse and forward shocks. The prospects for such a model for GRB 130427A are outlined in Vurm et al. (2014); they argue that the proposed blast wave model can be consistent with radio and hard X-ray data with reasonable assumptions regarding the reverse shock and nonthermal particle acceleration. Vurm et al. (2014) also pointed out the importance of using the correct mean molecular weight per electron, $\mu_e = 2$, expected for a Wolf-Rayet wind. The external density estimated from the late nonthermal optical flux scales as μ_e^3 . Using $\mu_e = 2$ instead of $\mu_e = 1$ increases the inferred parameter A by the factor of 8 and, at least in the case of GRB 130427A, makes it consistent with the value measured from the GeV flash.

We are grateful to Nicola Omodei for providing the LAT catalogue data, Antonio Martin-Carrillo for providing GRB 120711A data, and Tom Vestrand for providing GRB 130427A data. This work was supported by NSF grant AST-1412485, NASA ATP grant NNX15AE26G, and Swift Cycle 10 grant NNX14AI94G.

A. Analytical estimates

Here we summarize the analytical estimates derived in Beloborodov et al. (2014) to show basic trends in the flash model. Consider an idealized model of the prompt MeV radiation with a fixed spectrum and duration. One main parameter is left free — the prompt luminosity L_{GRB} .

The Lorentz factor and radius of the blast wave at the GeV peak are related to the observed peak time T_p by Equations (48) and (49) in Beloborodov et al. (2014),

$$\Gamma_p \approx 500 L_{54}^{3/13} \left(\frac{T_p}{1+z} \right)^{-3/13}, \quad (\text{A1})$$

$$R_p \approx 10^{16} L_{54}^{6/13} \left(\frac{T_p}{1+z} \right)^{7/13} \text{ cm}, \quad (\text{A2})$$

where $L_{54} = L_{\text{GRB}}/10^{54} \text{ erg s}^{-1}$ and T_p is measured in seconds. Note that the external density parameter A does not enter these relations; the values of R_p and Γ_p are controlled by pair loading $Z_{\pm}(R)$ which does not depend on density. The results of detailed simulations reported in Section 4 for our GRB sample show moderate deviations from the simplified relations (A1) and (A2).

The photon number emitted in the GeV flash (its isotropic equivalent) is estimated as

$$N_{\text{GeV}} \sim \frac{4\pi AR_p}{\mu_e m_p} Z_{\pm}(R_p) \mathcal{M}, \quad (\text{A3})$$

where

$$\mathcal{M}(E) \sim \frac{\Gamma_p m_e c^2}{(E_t E)^{1/2}} \quad (\text{A4})$$

is the average number of IC photons of energy $E \sim 1$ GeV emitted by a single post-shock electron, and $E_t \sim 1$ MeV is the typical energy of target prompt photons. Combining Equations (A1)–(A4), one can express the wind density parameter as

$$A_{11} \approx 0.3 N_{\text{GeV},56} L_{54}^{-9/13} \left[\frac{T_p}{1+z} \right]^{-4/13} \left[\frac{Z_{\pm}(R_p)}{10^4} \right]^{-1} \left(\frac{E_t}{1 \text{ MeV}} \right)^{1/2} \left(\frac{E}{1 \text{ GeV}} \right)^{1/2}, \quad (\text{A5})$$

where we have normalized the number of high-energy photons to the typical value $N_{\text{GeV}} \sim 10^{56}$ observed in our sample.

The kinetic luminosity of the ejecta L_{ej} can be roughly estimated assuming a relativistic reverse shock and a pressure balance between the reverse and forward shocks (see Beloborodov et al. 2014),

$$L_{\text{ej}} \sim 4 \times 10^{53} N_{\text{GeV},56} \left[\frac{T_p}{1+z} \right]^{-1} \left(\frac{E_t}{1 \text{ MeV}} \right)^{1/2} \left(\frac{E}{1 \text{ GeV}} \right)^{1/2} \text{ erg s}^{-1}. \quad (\text{A6})$$

If the reverse shock is not ultra-relativistic, equation (A6) should be considered as a lower limit.

Finally, if the simultaneous optical flash is detected, an estimate of the blast wave magnetization is given by (see Equation 81 in Beloborodov et al. 2014)

$$\epsilon_B \sim 3 \times 10^{-4} \left[\frac{Z_{\pm}(R_{\text{opt}})}{100} \right]^{-2} L_{\text{opt},49}^2 R_{\text{opt},16}^{-2} A_{11}^{-1} \left(\frac{L_{\text{GRB}}}{L_{\text{ej}}} \right)^2 \left(\frac{E_t}{1 \text{ MeV}} \right)^{-2} (1+z)^{-2}, \quad (\text{A7})$$

where $L_{\text{opt},49}$ is the peak luminosity of the optical flash normalized to 10^{49} erg s^{−1}, and R_{opt} is the radius where the optical flash peaks, which is slightly outside the peak radius of the GeV flash, R_p .

REFERENCES

- Abdo, A. A., Ackermann, M., Ajello, M., et al. 2009a, *ApJ*, 706, L138
- Abdo, A. A., Ackermann, M., Arimoto, M., et al. 2009b, *Science*, 323, 1688
- Ackermann, M., Asano, K., Atwood, W. B., et al. 2010, *ApJ*, 716, 1178
- Ackermann, M., Ajello, M., Asano, K., et al. 2011, *ApJ*, 729, 114
- . 2013a, *ApJ*, 763, 71
- . 2013b, *ApJS*, 209, 11
- . 2014, *Science*, 343, 42
- Aleksić, J., Alvarez, E. A., Antonelli, L. A., et al. 2012, *Astroparticle Physics*, 35, 435
- Aliu, E., Aune, T., Barnacka, A., et al. 2014, *ApJ*, 795, L3
- Beloborodov, A. M. 2002, *ApJ*, 565, 808
- . 2005, *ApJ*, 627, 346
- . 2010, *MNRAS*, 407, 1033
- Beloborodov, A. M., Hascoët, R., & Vurm, I. 2014, *ApJ*, 788, 36
- Crowther, P. A. 2007, *ARA&A*, 45, 177
- De Pasquale, M., Schady, P., Kuin, N. P. M., et al. 2010, *ApJ*, 709, L146
- Domínguez, A., Primack, J. R., Rosario, D. J., et al. 2011, *MNRAS*, 410, 2556
- Funk, S., Hinton, J. A., & CTA Consortium. 2013, *Astroparticle Physics*, 43, 348
- Gao, W.-H., Mao, J., Xu, D., & Fan, Y.-Z. 2009, *ApJ*, 706, L33
- Gehrels, N., Ramirez-Ruiz, E., & Fox, D. B. 2009, *ARA&A*, 47, 567
- Genet, F., Daigne, F., & Mochkovitch, R. 2007, *MNRAS*, 381, 732
- Ghirlanda, G., Nava, L., Ghisellini, G., et al. 2012, *MNRAS*, 420, 483
- Ghisellini, G., Ghirlanda, G., Nava, L., & Celotti, A. 2010, *MNRAS*, 403, 926
- Gilmore, R. C., Madau, P., Primack, J. R., Somerville, R. S., & Haardt, F. 2009, *MNRAS*, 399, 1694
- Goldstein, A., Burgess, J. M., Preece, R. D., et al. 2012, *ApJS*, 199, 19

- Golenetskii, S., Aptekar, R., Frederiks, D., et al. 2013, GRB Coordinates Network, 14487, 1
- Granot, J., Cohen-Tanugi, J., & do Couto e Silva, E. 2008, ApJ, 677, 92
- Greiner, J., Clemens, C., Krühler, T., et al. 2009, A&A, 498, 89
- Gruber, D., & Pelassa, V. 2012, GRB Coordinates Network, 13437, 1
- Hascoët, R., Beloborodov, A. M., Daigne, F., & Mochkovitch, R. 2014, ApJ, 782, 5
- Hascoët, R., Daigne, F., Mochkovitch, R., & Vennin, V. 2012, MNRAS, 421, 525
- He, H.-N., Wu, X.-F., Toma, K., Wang, X.-Y., & Mészáros, P. 2011, ApJ, 733, 22
- Hinton, J. A., & the HESS Collaboration. 2004, New A Rev., 48, 331
- Holder, J. 2011, International Cosmic Ray Conference, 12, 137
- Inoue, S., Granot, J., O’Brien, P. T., et al. 2013, Astroparticle Physics, 43, 252
- Kieda, D. B., Acciari, V. A. Aliu, E., & the VERITAS Collaboration. 2013, Proc. of 33rd ICRC, Rio de Janeiro, Brazil
- Kumar, P., & Barniol Duran, R. 2009, MNRAS, 400, L75
- Liang, E.-W., Yi, S.-X., Zhang, J., et al. 2010, ApJ, 725, 2209
- Lithwick, Y., & Sari, R. 2001, ApJ, 555, 540
- Martin-Carrillo, A., Hanlon, L., Topinka, M., et al. 2014, A&A, 567, A84
- Maxham, A., Zhang, B.-B., & Zhang, B. 2011, MNRAS, 415, 77
- Mészáros, P., & Rees, M. J. 1997, ApJ, 476, 232
- Panaitescu, A., Vestrand, W. T., & Woźniak, P. 2013, MNRAS, 436, 3106
- Pandey, S. B., Swenson, C. A., Perley, D. A., et al. 2010, ApJ, 714, 799
- Racusin, J. L., Oates, S. R., Schady, P., et al. 2011, ApJ, 738, 138
- Sironi, L., & Spitkovsky, A. 2011, ApJ, 726, 75
- Sitarek, J., Carmona, E., Colin, P., et al. 2013, Proc. of 33rd ICRC, Rio de Janeiro, Brazil
- Swenson, C. A., Maxham, A., Roming, P. W. A., et al. 2010, ApJ, 718, L14
- Thompson, C., & Madau, P. 2000, ApJ, 538, 105
- Uhm, Z. L., & Beloborodov, A. M. 2007, ApJ, 665, L93

- Vestrand, W. T., Wren, J. A., Panaitescu, A., et al. 2014, *Science*, 343, 38
- Vurm, I., Hascoët, R., & Beloborodov, A. M. 2014, *ApJ*, 789, L37
- Woosley, S. E., & Bloom, J. S. 2006, *ARA&A*, 44, 507
- Zou, Y.-C., Fan, Y.-Z., & Piran, T. 2009, *MNRAS*, 396, 1163

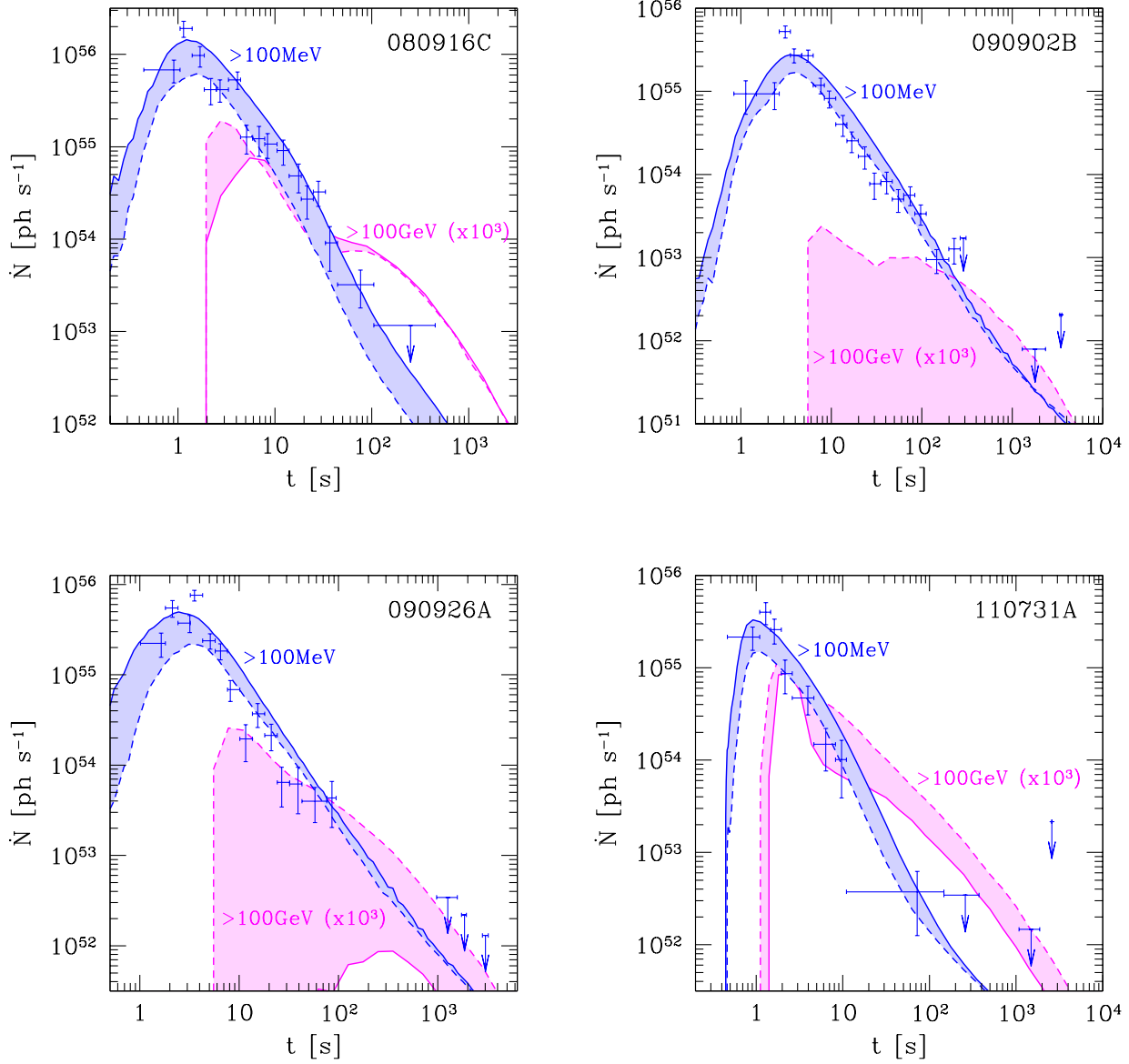


Fig. 1.— Model light curves and data for GRBs 080916C, 090902B, 090926A and 110731A. Theoretical photon flux (isotropic equivalent) and data above 100 MeV are shown in blue, and the photon flux predicted above 100 GeV is shown in magenta. Time t is measured in the rest frame of the central engine, $t = t_{\text{obs}}/(1+z)$. Solid curves show the high- A (high- Γ_{ej}) model and dashed curves show the low- A (low- Γ_{ej}) model (see Table 1).

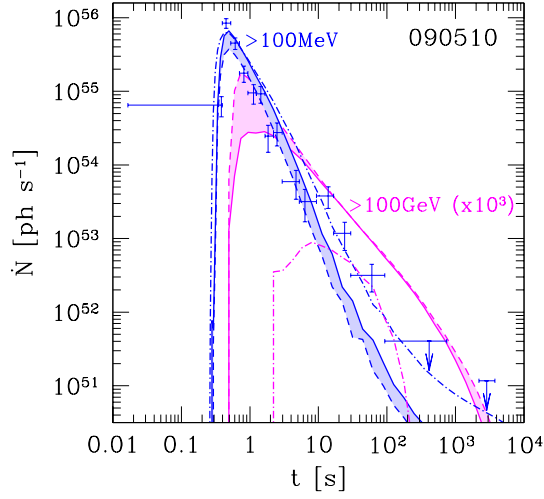


Fig. 2.— Model light curves and data for GRB 090510. Theoretical photon flux (isotropic equivalent) and data above 100 MeV are shown in blue, and the photon flux predicted above 100 GeV is shown in magenta. Time t is measured in the rest frame of the central engine, $t = t_{\text{obs}}/(1+z)$. Solid curves show the high- A (high- Γ_{ej}) model and dashed curves show the low- A (low- Γ_{ej}) model (see Table 1). The dashed-dotted curve shows the model with uniform external medium.

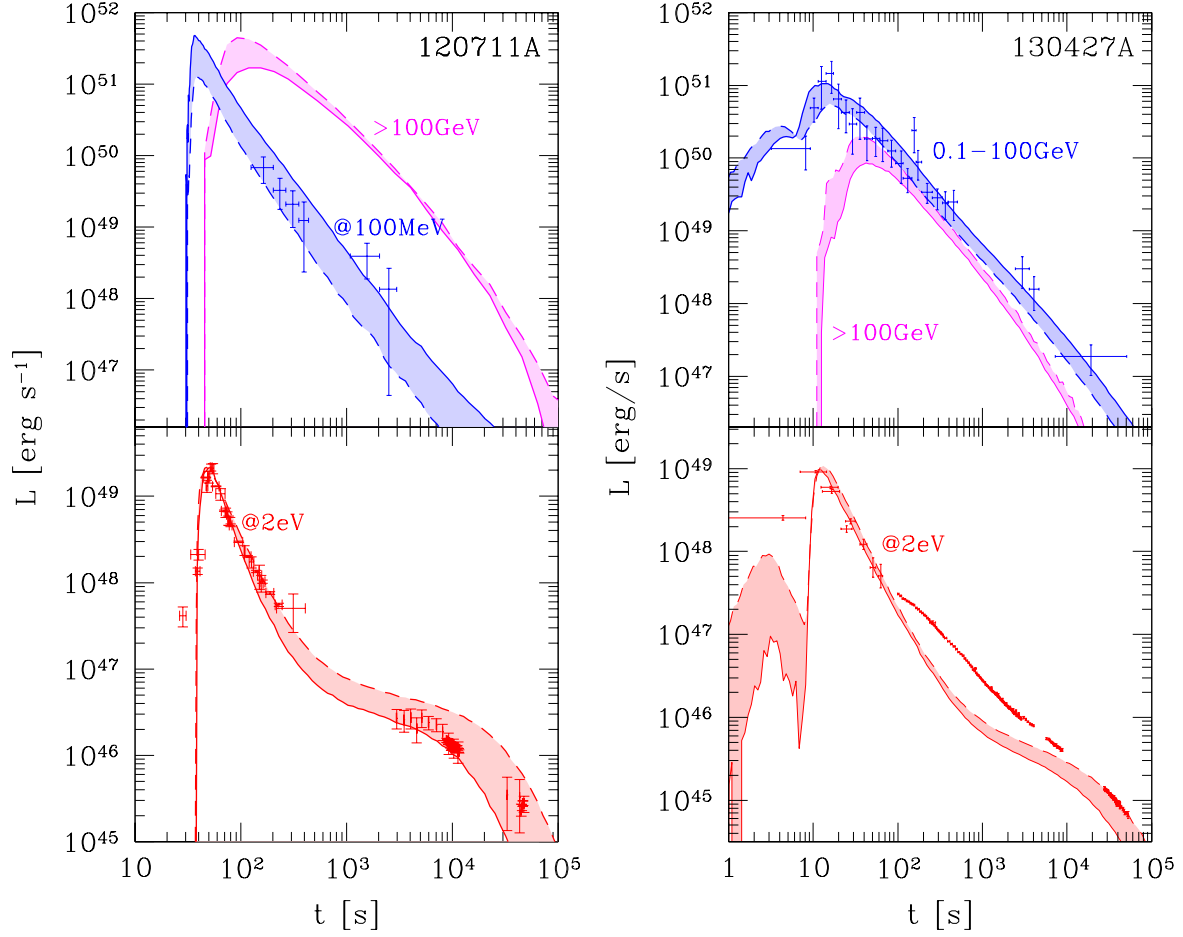


Fig. 3.— Model light curves and data for GRBs 120711A and 130427A. Solid curves show the high- A (high- Γ_{ej}) model and dashed curves show the low- A (low- Γ_{ej}) model (see Table 1). Upper panels: theoretical luminosity and data above 100 MeV (blue) and the luminosity predicted above 100 GeV (magenta). Lower panels: theoretical luminosity and data at 2 eV.

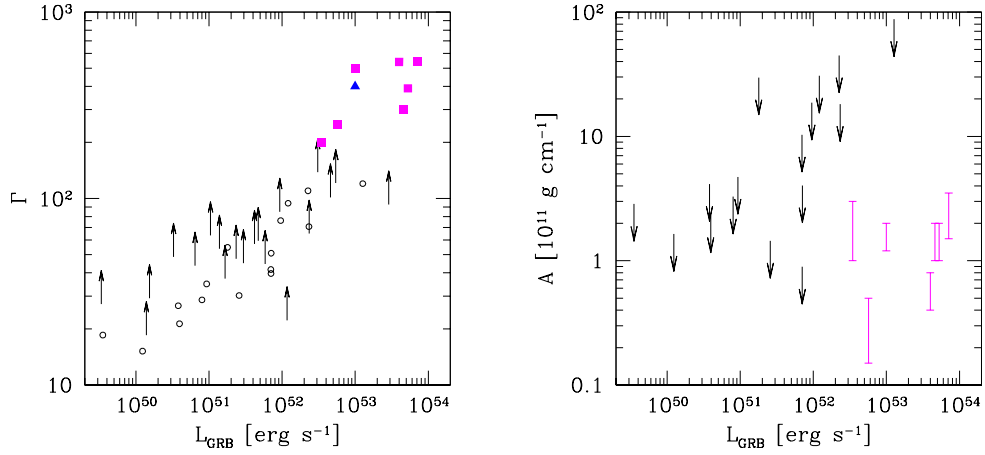


Fig. 4.— Left panel: blast wave Lorentz factor (before deceleration) versus the prompt GRB luminosity $L_{\text{GRB}} = E_{\text{GRB}}/T_{\text{GRB}}$. The 7 LAT bursts studied in this paper are plotted as magenta filled squares. We included the short GRB 090510 and modeled its GeV flash with both wind (magenta square) and uniform (blue triangle) external medium. For comparison, we also show the estimates (open circles) and lower limits (arrows) for Γ obtained for a sample of weaker bursts with a different method (Hascoët et al. 2014). Right panel: distribution of wind parameters in units of $10^{11} \text{ g cm}^{-1}$. The LAT bursts studied in this paper are plotted in magenta. Arrows show the upper-limits from Hascoët et al. (2014).